to be submitted to:
Nuclear Instruments & Methods in Physics Research B

Light Ion Double-Differential Cross Section Parameterization and Results from the SHIELD Transport Code

John W. Norbury[a], Liudmila Latysheva[b], Nikolai Sobolevsky[b]

[a] *NASA Langley Research Center, Hampton, Virginia, USA*
[b] *Institute for Nuclear Research of the Russian Academy of Sciences, Moscow, Russia*

Abstract
Light ions and neutrons have been shown to make large contributions to space radiation dose equivalent for realistic shielding scenarios. Efficient and accurate calculations of light ion double-differential cross sections are required for input into space radiation transport codes. A thermal proton cross section model is developed which includes proton production from the three sources of projectile, central fireball, and target. It is shown that this three-source model is able to explain the low momentum shoulder seen in proton spectra. Using the coalescence model, the thermal proton model is used to calculate light ion double-differential cross sections employed in space radiation transport codes. The three-source model is also seen to be essential to explain the light ion shoulders, which are even more pronounced than the proton shoulders. Comparisons are also made to the cross section models used in the SHIELD transport code.

1 Introduction

Future long duration space missions beyond low Earth orbit will continue to involve a large number of international partners. Many space agencies have modeling tools that can be used to evaluate space radiation effects, and a program has recently begun that compares the results of American (NASA) and Russian (ROSCOSMOS) space radiation codes. Five meetings have been held in Moscow, with other space agencies from Europe, Canada and Japan joining the last two meetings. Three papers [1, 2, 3] have already been published concerning work initiated at these meetings.

In the first paper [1], the space radiation transport codes, HZETRN (NASA) [4, 5, 6, 7, 8], SHIELD (ROSCOSMOS) [9, 10], FLUKA [11] and GEANT [12] were compared to each other for heavy ion, light ion[1], and pion production after the galactic cosmic ray (GCR) spectrum[2] was transported through various aluminum shield thicknesses. It was shown that the biggest differences among the codes occurred for light ion production in the low energy region below several hundred MeV. The disagreements were thought to be due to differences in nuclear models employed in the different codes. The second paper [2] focused on models of pion production cross sections used in the HZETRN (NASA) and SHIELD (ROSCOSMOS) transport codes. It was found that these models are in moderate agreement with each other and with experimental data, and further model improvements were recommended. The third paper [3] focused on calculation of the GCR environment flux. Commonly used GCR models were compared with recently published measurements of cosmic ray Hydrogen, Helium, and the Boron-to-Carbon ratio from the Alpha Magnetic Spectrometer (AMS). The models were developed and calibrated prior to the publication of the AMS data; therefore this was an opportunity to validate the models against an independent data set. Overall, the different GCR models were in reasonable agreement with AMS data in energy regions important for space radiation.

The present work represents the fourth paper in this series and is devoted to comparing NASA and ROSCOSMOS cross section models for light ion production. Recent work [13, 14] has shown that light ions and neutrons provide the dominant contribution to space radiation dose equivalent for realistic spacecraft shielding of about 20 g/cm^2 or more. This is in contrast to thinly shielded regions of about 5 g/cm^2 or less, where the dominant contribution comes from high linear energy transfer (LET) heavy ions.

As mentioned above, Norbury et al. [1] compared light ion and neutron production obtained by different transport techniques because of the importance of light ions and neutrons to astronaut exposure in realistic shielding scenarios. The largest differences between the various transport codes occurred for light ion production. Large differences for light ion production have also been seen in other transport code comparison studies

[1]Light ions are defined to be isotopes of Hydrogen (H) and Helium (He); ions heavier than He are called heavy ions.

[2]Galactic cosmic rays represent a continuous source of radiation that constitutes one of the major hazards during deep space exploration missions for both astronauts/cosmonauts and hardware.

[15] for thick 60 g/cm^2 targets. Furthermore, measurements of light ions on the Martian surface with the MSLRAD instrument show large differences between measurements and transport codes [16]. Finally, recent unpublished measurements [17] made at the NASA Space Radiation Laboratory (NSRL) with high energy, heavy ion transport through thick shielding targets show significant discrepancies between measurements and transport code predictions for light ion production. Consequently, light ion production is now considered to be the largest physics uncertainty in space radiation calculations.

Many transport codes, such as SHIELD [9, 10], FLUKA [11], GEANT [12], PHITS [18, 19], MCNP [20], and HETC [21, 22] employ stochastic Monte-Carlo (MC) techniques. However, NASA employs deterministic codes, such as HZETRN [23] and 3DHZETRN [4, 5, 6, 7, 8], which are highly computationally efficient as compared to MC codes and may be used for spacecraft design and real-time evaluation of space radiation environments. These deterministic codes require quick and efficient calculation of nuclear interaction cross sections. Cross sections can also be evaluated to a high degree of accuracy with MC techniques, but these are often too inefficient to be useful for deterministic transport. Consequently, specialized parameterizations are often developed for cross section calculations [24].

A consistent and important theme for verification and validation of the NASA deterministic transport codes has always involved comparisons of results with MC codes for simplified geometries that can be evaluated within a reasonable time frame [4, 5, 6, 7, 8]. This theme is continued in the present work with cross section models. A fast and efficient light ion double-differential cross section model parameterization developed for use in deterministic transport codes will be compared to cross section results used in the SHIELD Monte-Carlo code.

Light ions and neutrons scatter at both small and large angles as they undergo transport within spacecraft shielding. High energy heavy ions, however, typically continue moving in the forward direction due to their large forward momentum. One-dimensional deterministic transport codes [23] employing the straight-ahead approximation have been used successfully to describe the transport of high energy heavy ions. However, this approximation fails for large angle scattering of light ions and neutrons, and special three-dimensional deterministic transport codes have been developed to calculate light ion and neutron transport through spacecraft shielding [4, 5, 6, 7, 8]. These three-dimensional deterministic transport codes require double-differential cross sections as input. Efficient cross section parameterizations are required that are valid for all GCR projectile nuclei from Hydrogen to Nickel and for energies up to tens of GeV/n. While some double-differential cross section model parameterizations have been previously developed [25, 26, 27] for specific projectile-target combinations valid at certain energies, a model for all GCR projectile nuclei (up to Nickel) and all energies (tens of GeV/n), does not yet exist.

The present work seeks to develop model parameterizations of double-differential cross sections for light ion production in high energy nuclear collisions valid for the GCR nuclear

spectrum. The parameterizations are developed with the goal of efficient cross section calculations that can be used in fast, deterministic three-dimensional space radiation transport codes. Full details of the model can be found in an internal report [28], and the main highlights will be discussed herein. As discussed above, another goal of the present work is to provide a comparison to cross section models used in the Russian SHIELD (ROSCOSMOS) transport code [9, 10].

2 Parameterized double-differential cross section model

When a high energy projectile nucleus collides with a target nucleus, there are typically three states of matter produced, namely a projectile fragment $\mathcal{P}$, a target fragment $\mathcal{T}$, and a highly excited central $\mathcal{C}$ overlap region[3] involving pieces of both the projectile and target that have collided directly. All three regions subsequently decay, and all three sources can contribute to light ion fragment production measured in experiments.

Due to interest in specific fragment energies and production mechanisms, many early theoretical models [25, 26, 27, 29, 30] of the collision process considered only contributions to light ion production from either projectile fragmentation or central fireball emission. One of the first studies that considered adding contributions from both the projectile and central fireball for light ion production was performed by Auble et al. [25]; however, target contributions were not taken into account.

From the applied space radiation transport point of view, it is necessary to include fragments produced from all sources. There is no light ion double-differential cross section parameterization that exists for the complete GCR spectrum that includes production from all the three sources of projectile fragment, target fragment and central fireball: Such a parameterization is developed herein.

As the central fireball cools and decays it emits nucleons that coalesce into the light ion isotopes of H and He. The fireball density drops very rapidly, and nucleons are unable to coalesce to form heavier ions. Of course, the projectile and target fragments also emit nucleons and these can also coalesce. Thus, light ions are produced from nucleon coalescence of all three sources; projectile, central fireball and target[4].

2.1 Thermal proton production model

A double-differential cross section parameterization is now developed for proton production that will be valid for the GCR spectrum and include the three sources mentioned

[3]The central region is often called the fireball. It is typically much hotter and more excited than the projectile and target fragments.

[4]There will also be direct production of light ions, but this will not occur via fireball production, and target production will be limited to quite small momentum values, and so the dominant direct production source is the projectile fragment. Such direct production is seen mainly at very small angles [27], and is not necessary to explain the larger angle data of Nagamiya et al. [26] studied in the present work.

above. The model parameterization is based on a thermal model [26] for emitting an arbitrary type of particle fragment.

2.1.1 Single-source model

The thermal model expression for the Lorentz-invariant double-differential cross section for production of a fragment particle is [26]

$$E\frac{d^3\sigma}{dp^3} = N\, e^{-T/\Theta} \,, \tag{1}$$

where T is the kinetic energy of the emitted fragment. The temperature Θ is given in units of energy and N is a constant. Equation (1) seems very simple, but its practical implementation is more complicated, as seen later in equation (18).

The constant N is related to the total cross section σ. However, it is often simply fitted to data [25, 26]; this is unsatisfactory for the model parameterization being developed herein for use in transport codes. Instead, N will be evaluated correctly in terms of σ, which is the integral of the Lorentz-invariant differential cross section,

$$\sigma \equiv \int \frac{d^3p}{E}\left(E\frac{d^3\sigma}{dp^3}\right) = 4\pi\int_0^\infty dp\frac{p^2}{E}\left(E\frac{d^3\sigma}{dp^3}\right) = 4\pi\int_0^\infty dT\sqrt{T(T+2m)}\left(E\frac{d^3\sigma}{dp^3}\right) \,, \tag{2}$$

with the 4π factor arising from assuming isotropic emission of particles in the reference frame in which they are produced. Inserting the thermal model of equation (1) gives

$$\sigma = 4\pi N\int_0^\infty dT\sqrt{T(T+2m)}\; e^{-T/\Theta} \,. \tag{3}$$

Using the result

$$\int_0^\infty dT\sqrt{T(T+2m)}\; e^{-T/\Theta} = m\Theta e^{m/\Theta}K_1(m/\Theta) \,, \tag{4}$$

where $K_1(m/\Theta)$ is the modified Bessel function of the second kind [31] of order 1 as a function of m/Θ, giving the thermal model total cross section as

$$\sigma = 4\pi N m\Theta e^{m/\Theta}K_1(m/\Theta). \tag{5}$$

Substituting into equation (1), gives the single-source thermal model (correctly normalized so that the integral of the Lorentz-invariant differential cross section gives the total cross section), which becomes

$$E\frac{d^3\sigma}{dp^3} = \frac{\sigma}{4\pi m\Theta K_1(m/\Theta)}\; e^{-(T+m)/\Theta} \,. \tag{6}$$

2.1.2 Three-source model

As mentioned previously, the cross section measured in the lab frame will contain contributions from the projectile fragment, the central fireball and the target fragment. Note that the target is approximately at rest in the lab frame. Therefore, the target rest frame is considered identical to the lab rest frame. Cross sections from each of these three frames must be Lorentz-transformed to the lab frame and added together to form the final lab frame cross section. The lab frame is also identical with the spacecraft rest frame through which GCR particles are transported. In any particle production cross section model, including thermal models, there will be contributions from all three sources.

One might use the symbols $\mathcal{P}$, $\mathcal{C}$, or $\mathcal{T}$ for the projectile, central fireball or target rest frames respectively. However, the general expressions for the Lorentz-transformations will be the same for any frame and so a more compact notation using the $*$ symbol will be used, where $*$ refers to any of the projectile, central fireball, or target rest frames. The symbols $\mathcal{P}$, $\mathcal{C}$, or $\mathcal{T}$ will only be used if it is necessary to specify a particular frame.

Equation (1) is the general expression for a thermal model cross section evaluated in any of the three source frames discussed previously. The thermal model for a particle j emitted in the $*$ frame ($*$ = projectile $\mathcal{P}$, or central fireball $\mathcal{C}$, or target $\mathcal{T}$) is

$$\left[E\frac{d^3\sigma}{dp^3}(p_{jL},\theta_{jL})\right]_* = N\, e^{-T_{j*}/\Theta_*} = N\, \exp[-T_{j*}(p_{jL},\theta_{jL})/\Theta_*]\ , \tag{7}$$

where p_{jL} and θ_{jL} are the momentum and angle of particle j in the lab frame, L. The notation (p_{jL},θ_{jL}) indicates that the functions must be written as explicit functions of the lab frame L variables p_{jL} and θ_{jL} because these are the variables used for the experimental cross sections, with which the thermal model is to be compared. However, T_{j*} is the kinetic energy of particle j in the $*$ frame, and this needs to be Lorentz-transformed to the lab frame L. The temperature of the $*$ frame is Θ_*, which does not need to be Lorentz-transformed because it is a Lorentz-scalar.

In order to Lorentz-transform the particle j kinetic energy T, write

$$T_{j*} \equiv E_{j*} - m_j\ , \tag{8}$$

where E is the total energy and m is the rest mass[5] energy. The Lorentz-transformation of the total energy is [32]

$$E_{j*} = \gamma_{*L}\, E_{jL} - \gamma_{*L}\, \beta_{*L}\, p_{ZjL}\ , \tag{9}$$

where the longitudinal momentum is given as $p_{ZjL} \equiv p_{jL}\cos\theta_{jL}$, with $p_{jL} \equiv |\mathbf{p}_{jL}|$. The relativistic γ_{*L} and β_{*L} factors refer to the speed[6] of the $*$ frame with respect to the lab

[5]Standard particle physics units are used throughout this paper with the speed of light $c \equiv 1$.

[6]The speed of the projectile, relative to the lab, is easily determined from the projectile kinetic energy. The speed of the target, relative to the lab, is zero. The approach used in the present work is to take the central fireball speed to be identical to the speed of the nucleon-nucleon center-of-momentum rest frame, as in the study of Nagamiya et al. [26].

frame L. That is, they are relations *between* different reference frames and have nothing to do with particle j. Thus, the Lorentz-transformed total energy of particle j in terms of (p_{jL}, θ_{jL}) variables is

$$E_{j*} = \gamma_{*L} \sqrt{p_{jL}^2 + m_j^2} - \gamma_{*L}\ \beta_{*L}\ p_{jL} \cos\theta_{jL}\ , \tag{10}$$

which is simply substituted into equation (7) via equation (8) to give the final answer for the thermal model Lorentz-invariant double-differential cross section in the $*$ frame,

$$\left[E\frac{d^3\sigma}{dp^3}(p_{jL}, \theta_{jL})\right]_* = N\ \exp[-(\gamma_{*L} \sqrt{p_{jL}^2 + m_j^2} - \gamma_{*L}\ \beta_{*L}\ p_{jL} \cos\theta_{jL} - m_j)/\Theta_*]\ . \tag{11}$$

Once one has the right hand side of the Lorentz-invariant differential cross section of equation (7) written explicitly in terms of the lab L, variables (p_{jL}, θ_{jL}), then one has the final answer as equation (11), which is the $*$ frame Lorentz-invariant differential cross section in terms of particle j lab frame variables (p_{jL}, θ_{jL}). The left hand side of equation (7) or (11) in terms of (p_{jL}, θ_{jL}) variables is the $*$ frame Lorentz-invariant differential cross section, which is equal to the lab frame Lorentz-invariant differential cross section precisely because the quantity $E\frac{d^3\sigma}{dp^3}$ is Lorentz-invariant.

Cross sections for j particles from the three sources need to be added together as

$$\begin{aligned} E\frac{d^3\sigma}{dp^3}(p_{jL}, \theta_{jL}) &= \left[E\frac{d^3\sigma}{dp^3}(p_{jL}, \theta_{jL})\right]_{\mathcal{P}} + \left[E\frac{d^3\sigma}{dp^3}(p_{jL}, \theta_{jL})\right]_{\mathcal{C}} + \left[E\frac{d^3\sigma}{dp^3}(p_{jL}, \theta_{jL})\right]_{\mathcal{T}} \\ &= N\,(e^{-T_{jL}/\Theta_{\mathcal{P}}} + e^{-T_{jL}/\Theta_{\mathcal{C}}} + e^{-T_{jL}/\Theta_{\mathcal{T}}})\ . \end{aligned} \tag{12}$$

The cross sections can be added in this simple way because they are all Lorentz-invariant. Each of the three terms in equation (12) is calculated using equation (11), where $*$ is replaced by $\mathcal{P}$, $\mathcal{C}$, or $\mathcal{T}$ symbols representing projectile, central fireball, or target, respectively. (Of course, the target frame is identical to the lab frame, so that the Lorentz-transformation is trivial, in that $\gamma_{\mathcal{T}L} = 1$ and $\beta_{\mathcal{T}L} = 0$, resulting in the identity $E_{j\mathcal{T}} = E_{jL}$.) Explicitly, equations (11) and (12) give

$$\begin{aligned} E\frac{d^3\sigma}{dp^3}(p_{jL}, \theta_{jL}) &= N\{\exp[-(\gamma_{\mathcal{P}L} \sqrt{p_{jL}^2 + m_j^2} - \gamma_{\mathcal{P}L}\ \beta_{\mathcal{P}L}\ p_{jL} \cos\theta_{jL} - m_j)/\Theta_{\mathcal{P}}] \\ &\quad + \exp[-(\gamma_{\mathcal{C}L} \sqrt{p_{jL}^2 + m_j^2} - \gamma_{\mathcal{C}L}\ \beta_{\mathcal{C}L}\ p_{jL} \cos\theta_{jL} - m_j)/\Theta_{\mathcal{C}}] \\ &\quad + \exp[-(\gamma_{\mathcal{T}L} \sqrt{p_{jL}^2 + m_j^2} - \gamma_{\mathcal{T}L}\ \beta_{\mathcal{T}L}\ p_{jL} \cos\theta_{jL} - m_j)/\Theta_{\mathcal{T}}]\}. \end{aligned} \tag{13}$$

This equation represents the thermal model with contributions from the projectile, target and central sources, all Lorentz-transformed to the lab frame; equation (13) is the practical implementation of the simple-looking form of the thermal model in equation (1).

Next, the normalization constant N must be evaluated. For the three-source thermal model, the normalization is more complicated than for the single-source normalization in equation (6). The total cross section is obtained by integrating all three sources. Using equation (12) and following the method of equation (2) gives

$$\begin{aligned}
\sigma &\equiv \int \frac{d^3p}{E}\left(E\frac{d^3\sigma}{dp^3}\right) \\
&= \int \frac{d^3p}{E}\left\{\left[E\frac{d^3\sigma}{dp^3}(p_{jL},\theta_{jL})\right]_{\mathcal{P}} + \left[E\frac{d^3\sigma}{dp^3}(p_{jL},\theta_{jL})\right]_{\mathcal{C}} + \left[E\frac{d^3\sigma}{dp^3}(p_{jL},\theta_{jL})\right]_{\mathcal{T}}\right\} \\
&= 4\pi\int_0^\infty dp\frac{p^2}{E}\left\{\left[E\frac{d^3\sigma}{dp^3}(p_{jL},\theta_{jL})\right]_{\mathcal{P}} + \left[E\frac{d^3\sigma}{dp^3}(p_{jL},\theta_{jL})\right]_{\mathcal{C}} + \left[E\frac{d^3\sigma}{dp^3}(p_{jL},\theta_{jL})\right]_{\mathcal{T}}\right\} ,
\end{aligned} \tag{14}$$

so that

$$\begin{aligned}
\sigma &= 4\pi\int_0^\infty dT\sqrt{T(T+2m)} \\
&\quad\times\left\{\left[E\frac{d^3\sigma}{dp^3}(p_{jL},\theta_{jL})\right]_{\mathcal{P}} + \left[E\frac{d^3\sigma}{dp^3}(p_{jL},\theta_{jL})\right]_{\mathcal{C}} + \left[E\frac{d^3\sigma}{dp^3}(p_{jL},\theta_{jL})\right]_{\mathcal{T}}\right\} \\
&= 4\pi N\int_0^\infty dT_{jL}\sqrt{T_{jL}(T_{jL}+2m_j)}\,(e^{-T_{jL}/\Theta_{\mathcal{P}}} + e^{-T_{jL}/\Theta_{\mathcal{C}}} + e^{-T_{jL}/\Theta_{\mathcal{T}}}) \\
&= 4\pi N m_j\left[\Theta_{\mathcal{P}}e^{m_j/\Theta_{\mathcal{P}}}K_1(m_j/\Theta_{\mathcal{P}}) + \Theta_{\mathcal{C}}e^{m_j/\Theta_{\mathcal{C}}}K_1(m_j/\Theta_{\mathcal{C}}) + \Theta_{\mathcal{T}}e^{m_j/\Theta_{\mathcal{T}}}K_1(m_j/\Theta_{\mathcal{T}})\right] ,
\end{aligned} \tag{15}$$

giving the normalization

$$N = \frac{\sigma}{4\pi m_j\left[\Theta_{\mathcal{P}}e^{m_j/\Theta_{\mathcal{P}}}K_1(m_j/\Theta_{\mathcal{P}}) + \Theta_{\mathcal{C}}e^{m_j/\Theta_{\mathcal{C}}}K_1(m_j/\Theta_{\mathcal{C}}) + \Theta_{\mathcal{T}}e^{m_j/\Theta_{\mathcal{T}}}K_1(m_j/\Theta_{\mathcal{T}})\right]} . \tag{16}$$

The full three-source thermal model, correctly normalized so that the integral of the Lorentz-invariant differential cross section gives the total cross section, therefore becomes

$$\begin{aligned}
E\frac{d^3\sigma}{dp^3}(p_{jL},\theta_{jL}) &= \left[E\frac{d^3\sigma}{dp^3}(p_{jL},\theta_{jL})\right]_{\mathcal{P}} + \left[E\frac{d^3\sigma}{dp^3}(p_{jL},\theta_{jL})\right]_{\mathcal{C}} + \left[E\frac{d^3\sigma}{dp^3}(p_{jL},\theta_{jL})\right]_{\mathcal{T}} \\
&= \frac{\sigma(e^{-T_{jL}/\Theta_{\mathcal{P}}} + e^{-T_{jL}/\Theta_{\mathcal{C}}} + e^{-T_{jL}/\Theta_{\mathcal{T}}})}{4\pi m_j\left[\Theta_{\mathcal{P}}e^{m_j/\Theta_{\mathcal{P}}}K_1(m_j/\Theta_{\mathcal{P}}) + \Theta_{\mathcal{C}}e^{m_j/\Theta_{\mathcal{C}}}K_1(m_j/\Theta_{\mathcal{C}}) + \Theta_{\mathcal{T}}e^{m_j/\Theta_{\mathcal{T}}}K_1(m_j/\Theta_{\mathcal{T}})\right]} .
\end{aligned} \tag{17}$$

In terms of total 3-momentum and angle variables (p_{jL}, θ_{jL}), the final thermal model for proton production is

$$\begin{aligned} E\frac{d^3\sigma}{dp^3}(p_{jL},\theta_{jL}) &= \frac{\sigma}{4\pi m_j}\{\exp[-(\gamma_{\mathcal{P}L}\sqrt{p_{jL}^2+m_j^2}-\gamma_{\mathcal{P}L}\,\beta_{\mathcal{P}L}\,p_{jL}\cos\theta_{jL}-m_j)/\Theta_{\mathcal{P}}] \\ &\quad +\exp[-(\gamma_{\mathcal{C}L}\sqrt{p_{jL}^2+m_j^2}-\gamma_{\mathcal{C}L}\,\beta_{\mathcal{C}L}\,p_{jL}\cos\theta_{jL}-m_j)/\Theta_{\mathcal{C}}] \\ &\quad +\exp[-(\gamma_{\mathcal{T}L}\sqrt{p_{jL}^2+m_j^2}-\gamma_{\mathcal{T}L}\,\beta_{\mathcal{T}L}\,p_{jL}\cos\theta_{jL}-m_j)/\Theta_{\mathcal{T}}]\} \\ &\quad \times\left\{\Theta_{\mathcal{P}}e^{m/\Theta_{\mathcal{P}}}K_1(m_j/\Theta_{\mathcal{P}})+\Theta_{\mathcal{C}}e^{m_j/\Theta_{\mathcal{C}}}K_1(m_j/\Theta_{\mathcal{C}})+\Theta_{\mathcal{T}}e^{m_j/\Theta_{\mathcal{T}}}K_1(m_j/\Theta_{\mathcal{T}})\right\}^{-1}. \end{aligned} \tag{18}$$

This very nice, compact equation parameterizing the Lorentz-invariant double-differential proton thermal model cross section has not previously appeared in the literature[7]. It includes all three sources and is normalized correctly to the total cross section.

2.1.3 Total cross section values

Equations (6, 17, 18) give the Lorentz-invariant double-differential cross section for proton production, with normalization such that the integral of the differential cross section gives the total cross section, σ. Therefore, a separate model is needed to calculate σ. The present work uses the NUCFRG3 [24] model, but any other type of model could be used. Calculations for proton strong interaction production cross sections from nucleus-nucleus reactions are listed in Table 1. For the Ar + KCl and C + C reactions, the contributions from electromagnetic dissociation interactions are small [39, 40] and are not included here.

2.1.4 Temperature parameters

The entire set of models developed in the present work use only two adjustable parameters, which are the participant (central fireball) and spectator (projectile or target) temperatures. These are summarized in Table 2.

As mentioned previously, the nucleus-nucleus reaction contains two spectator pre-fragments, namely the projectile and target, as well as a participant region which is the central fireball. From the center-of-momentum frame it makes sense for both spectators to have the same temperature, given that temperature is a Lorentz-scalar. The participant region will be much hotter than the spectators. Values for these parameters are listed in Table 2. The choices were guided from values listed in the literature [26].

[7]Nevertheless, forms similar to equation (13) have appeared previously in the form of neutron production parameterizations [33, 34, 35, 36, 37, 38], where the cross section normalization N remains an adjustable parameter. None of the neutron parameterizations [33, 34, 35, 36, 37, 38] have written N in terms of the total cross section, as presented in equation (18). When N is treated as an adjustable parameter, there is no guarantee that the integrated double differential cross section correctly gives the total cross section.

2.2 Composite light ion coalescence model

A coalescence model, based on the work of Nagamiya et al. [26], is now developed for composite light ion (^{2,3}H, ^{3,4}He) production cross sections. The light ion Lorentz-invariant double-differential cross section $E_A\, d^3\sigma_A/dp_A^3$ is related to the proton Lorentz-invariant double-differential cross section $E_{\rm p}\, d^3\sigma_{\rm p}/dp_{\rm p}^3$ as [26]

$$E_A \frac{d^3\sigma_A}{dp_A^3} = C_A \left(E_{\rm p} \frac{d^3\sigma_{\rm p}}{dp_{\rm p}^3} \right)^A , \qquad \text{with} \;\; p_A \equiv A p_{\rm p} \;\; \text{and} \;\; E_A \equiv A E_{\rm p} \, , \tag{19}$$

where E and $p \equiv |\mathbf{p}|$ are the energy and 3-momentum magnitude of the emitted fragment, and dp^3 is the momentum volume element. A is the mass number of the light ion fragment and the p and A subscripts refer to a proton or light ion respectively. C_A is the coalescence model coefficient. The cross sections in equation (19) refer to light ion and proton fragment production for an arbitrary projectile and target. For example, if the reaction being considered is Fe (1 GeV/n) + Al, the ^{3}He production cross section on the left hand side of equation (19) refers to Fe (1 GeV/n) + Al $\rightarrow$ ^{3}He +X, (where X are other produced fragments), with the proton (p) production cross section on the right hand side of equation (19) referring to Fe (1 GeV/n) + Al $\rightarrow$ p + X.

Note that in equation (19) the units of the light ion energy and momentum are GeV, not GeV/n. This is an essential feature when using the proton cross sections on the right hand side of equation (19) as input. The coalescence model gives the energy and momentum of the light ion as $p_A \equiv A p_{\rm p}$ and $E_A \equiv A E_{\rm p}$ respectively. (However, if a transport code requires GeV/n, the conversion is trivial.)

The coalescence model of equation (19) is used to make predictions for light ion double-differential cross sections using the thermal model for the proton double-differential cross section, as given by equation (18). That is, equation (18) is used as input to the right hand side of equation (19), by summing each source and then raising the entire sum to the power A. In terms of (p_{jL}, θ_{jL}) variables, this becomes

$$E_A \frac{d^3\sigma_A}{dp_A^3} = C_A \left\{ \left[E \frac{d^3\sigma}{dp^3}(p_{jL}, \theta_{jL}) \right]_{\mathcal{P}} + \left[E \frac{d^3\sigma}{dp^3}(p_{jL}, \theta_{jL}) \right]_{\mathcal{C}} + \left[E \frac{d^3\sigma}{dp^3}(p_{jL}, \theta_{jL}) \right]_{\mathcal{T}} \right\}^A , \tag{20}$$

which is the model[8] used in the present work.

[8]The reason that the whole term is raised to a power, rather than raising each term individually, is that the coalescence model, as given in equation (19), raises the entire proton cross section to the power A. Theoretically the proton cross section is the sum of the 3 sources. Thus, the coalescence model implies that each source should be added first and then afterwards the entire sum is raised to the power A. Nevertheless, the idea of raising each term separately to the power A was thoroughly investigated and found to give significantly poorer agreement with experiment.

2.2.1 Coalescence coefficient

Observed [26] and calculated coalescence coefficients C_A are shown in Table 3. The observed values are taken from Table VIII in the paper of Nagamiya et al. [26]. The calculations also follow the method outlined by Nagamiya et al. [26] and proceed as follows. The coalescence coefficient C_A is calculated as [26]

$$C_A = \frac{c_A}{V^{A-1}} \,, \tag{21}$$

where c_A is a constant for each value of A, i.e. it is a constant which changes only if the mass number A of the produced fragment changes. Equation (21) is actually the non-relativistic limit of the coefficient in reference [26]. This is sufficient due to the very weak energy dependence of C_A, as seen in Table VIII of reference [26]. The interaction volume is $V = \frac{4}{3}\pi R^3$, with the interaction radius R given by [26]

$$R = a(A_{\mathcal{P}}^{1/3} + A_{\mathcal{T}}^{1/3}) + b \,, \tag{22}$$

where a and b are constants from reference [26] and $A_{\mathcal{P}}$ and $A_{\mathcal{T}}$ are the mass numbers of the projectile and target nuclei, respectively.

The calculated C_A values in equation (21) require the constant c_A values as input. These c_A are constants, which vary only with A. That is, c_A takes three different values (see Table 4) depending on whether the fragment is ^{2}H, ^{3}H, ^{3}He, ^{4}He, with the value for ^{3}H and ^{3}He being the same because the A number ($A = 3$) is the same. The values of c_A are *not* discussed in reference [26], and therefore, in the present work, they have been determined from the reaction Ar (800MeV/n) + KCl as follows,

$$c_A = C_A^{\mathrm{obs[Ar(800MeV/n)+KCl]}}\, V^{A-1} \,, \tag{23}$$

where $C_A^{\mathrm{obs[Ar(800MeV/n)+KCl]}}$ are the observed C_A values (see Table 3) for the reaction of Ar (800MeV/n) + KCl [26]. The reason that a single reaction can be chosen to determine c_A is that c_A values are the same for all reactions producing the same fragment. The Ar (800MeV/n) + KCl reaction was chosen because it includes observed values for ^{4}He, which are missing for other reactions (see Table 3). Values[9] for c_A are listed in Table 4, showing that the only dependence is on the light ion fragment mass number A. Only the *three* values in Table 4 are used for calculation of the *entire* set of reactions in Table 3, and for *all other* light ion cross section predictions. Note that both of these calculated quantities are independent of projectile kinetic energy, as seen in Table 3. Also, they have the same value for the same mass number A, so that values for ^{3}H and ^{3}He are the same, as also seen in Table 3.

[9] As already stated, c_A depends on the A number of the fragment produced, whereas it is misleadingly written simply as c (independent of A) in the work of reference [26].

3 SHIELD

To calculate Lorentz-invariant differential cross sections of light nuclei with the Russian (ROSCOSMOS) models, the generator of inelastic nuclear interactions, MSDM (Multi-Stage Dynamical Model) of the SHIELD transport code was used. The MSDM generator [41] includes current versions of well-known Russian models of nuclear reactions, and may be used separately, as a multipurpose Monte Carlo model of nuclear reactions.

The fast,cascade stage of nuclear reactions at energies below 1 GeV/n, is modeled using the Dubna intranuclear cascade model [42]. Above 10 GeV/n, the Quark-Gluon String Model (QGSM) [43] is used, while in the intermediate range 1 - 10 GeV/n, some extensions of QGSM [44] is used. Thus, a consistent description of the fast stage of nuclear reactions in the whole energy range of primary hadrons and nuclei up to 1 TeV/n is provided. By the end of the cascade stage, secondary nucleons close to each other in momentum space can coalesce to form a complex particle. Formation of fast deuterons, tritons, helions and alpha particles is possible during the coalescence stage [42].

Evolution of the excited residual nucleus into an equilibrium state is described in terms of the pre-equilibrium model based on the Monte Carlo solution of the corresponding Master equation [45]. Further equilibrium de-excitation of the residual nucleus includes several mechanisms. For light nuclei ($A < 16$), the modified model of Fermi break-up [46] is applied. Medium and heavy nuclei at moderate excitations ($E^* < 2$ MeV/n) de-excite themselves by particle evaporation [46]. For heavy nuclei, a competition of evaporation and fission is implemented [47]. Highly excited nuclei ($E^* > 2$ MeV/n) may decay into several excited fragments according to the Statistical Multi-fragmentation Model (SMM) [48] followed by the emission of particles from fragments. Thus, the MSDM generator provides description of all the stages of a nuclear reaction in the exclusive approach.

4 Comparison to experiment

The parameterized models and SHIELD cross sections are now compared to the Lorentz-invariant double-differential cross section data of Nagamiya et al. [26], for light ion production from Ar + KCl and C + C reactions, both with projectile kinetic energy of 800 MeV/n. Protons and composite light ions will be treated separately, since the parameterized model consists of a proton thermal model, used as input for the composite light ion coalescence model parameterization, as discussed previously.

This work examines 47 different data sets, summarized in Table 5. The complete number of data points is over 1,000. The proton production parameterization model only has the two temperature parameters, and the light ion coalescence parameterization model has no adjustable parameters. The combined proton - thermal and light ion - coalescence parameterized models are able to approximately predict over 1,000 data points based on only these two temperature parameters.

4.1 Protons

The proton production thermal model Lorentz-invariant double-differential cross sections, as given in equation (18), for Ar + KCl and C + C reactions are shown in Figures 1 and 2 respectively. Both reactions have projectile kinetic energy of 800 MeV/n. Figures 1 and 2 show total (red) and individual contributions from central fireball (blue), projectile (orange), and target (purple) for the parameterized thermal model. The figures show protons being produced at various angles in the lab frame. The total (red) result is to be compared to data.

The relative contributions of the projectile (orange), target (purple), and central fireball (blue) are interesting to study as the proton production angle changes. Thermal model production of protons is assumed to be isotropic in the frame in which the protons are produced. While the projectile and central fireball proton contributions vary, the target contribution remains the same as the angle changes. This is expected because the lab frame in which the momentum and angle of the proton are measured is identical to the target frame, and no Lorentz-transformation is required, since the speed of the target frame with respect to the lab is $\beta_{\mathcal{T}L} = 0$.

At intermediate angles (10° - 20°), Figures 1 and 2 show that projectile protons contribute the most at large proton momenta, with central fireball protons contributing most at intermediate momenta. This is because the projectile is moving much faster than the central fireball, even though the fireball is hotter. Because the fireball is so hot it also makes contributions at large momenta. At very small momenta the target contribution is large. As the proton production angle increases, the projectile contribution becomes smaller because projectile protons are mainly boosted in the forward direction and only very high energy thermal protons can exit at larger angles; therefore, at the largest angles the projectile contribution is negligible. At intermediate angles, central fireball production of protons is dominant. At the largest angles, only central fireball protons of very high energy can reach large angles in the lab frame, and so the central fireball protons contribute less, with target protons contributing a large amount at large angles.

The total proton results in Figures 1 and 2 are to be compared to the experimental data. While pion production cross sections show a smooth exponential fall-off with increasing momenta [2, 49, 50], due to dominant production from the central fireball, the proton cross sections show a significantly different behavior at intermediate angles between 10° - 20°. The dominant intermediate angle feature is a flat shoulder region that can be seen at lower momenta. This is seen not only in the proton spectra (Figures 1 and 2), but also in the composite light ion spectra (Figures 3 - 9). This shoulder feature was the main reason for introducing the parameterized model of the present work to include projectile, fireball, and target contributions. For pion cross sections, only a central fireball thermal model is all that is necessary to fit the data [2, 49, 50], whereas the shoulder region in the proton and light ion data necessitated the development of the present three-source model.

One of the main results of the present work is to show that the shoulder region of Figures 1 and 2 can be reproduced by summing projectile and fireball contributions from the parameterized thermal model. One of the first papers to develop this idea was by Auble et al. [25]. In summary, Figures 1 and 2 show that the proton spectral data can be reasonably reproduced with the three-source thermal proton model parameterization developed herein. Nevertheless, there is room for improvement: The thermal model shows some discrepancies with data at larger angles and higher lab momenta. This could perhaps be improved by a better choice of parameters, which will be examined in future work when comparison to a more extensive data set will be studied.

The cross section model results for proton production used in the SHIELD code are also shown in Figures 1 and 2. Comparisons with data are excellent and are, in general, better than the parameterized thermal model discussed previously. Exceptions are for the Ar +KCl reaction at 10° and 15°, where the SHIELD results over-estimate the shoulder region near 1.5 GeV and the parameterized thermal model is much closer to data.

4.2 Composite light ions

The light ion production coalescence parameterized model for Lorentz-invariant double-differential cross sections for Ar + KCl and C + C reactions are shown in Figures 3 - 9 compared to experimental data [26]. As with the proton cross sections, the light ion figures show total (red) and separated contributions from central fireball (blue), projectile (orange), and target (purple) from the parameterized model, with the relative kinematic contributions of the three sources showing similar angular behavior to the proton cross sections, discussed previously. Note however, that rather than a simple addition, individual contributions for composite light ions add according to equation (20). The separated contributions are calculated from equation (19) for *each individual source*. The separated contributions are shown for illustrative purposes only; unlike the case for protons, they do *not* simply add to give the total.

Similar conclusions regarding the relative contributions of projectile and central fireball as a function of angle were also discussed by Auble et al. [25]. At intermediate angles, the low-momentum shoulder region of the spectra is even more pronounced for light ions compared to protons, and the addition of the three sources is essential to explain the light ion shoulders. Overall, the light ion parameterized model provides a reasonable characterization of the experimental data. Nevertheless, as with the proton data, there is room for improvement, especially for triton and helion production from C + C reactions. More accurate calculation of the coalescence coefficients may improve the model.

Further validation of the composite light ion parameterized coalescence model is shown in Table 3. The calculated coalescence coefficients C_A and interaction radii R, listed in Table 3, are seen to be in reasonable agreement with the observed values. This provides some justification that the present light ion cross section model parameterization (for large angle light ion fragment production) developed herein is applicable to the wider

range of nuclei and energies in the GCR spectrum.

The cross section model results for composite light ion production used in the SHIELD code are also shown in Figures 3 - 9. For Ar + KCl reactions (Figures 3 - 6), the SHIELD results are excellent, except with a small over-estimate of the shoulder at 10° for detuerons and under-prediction of alpha cross sections. The C + C results (Figures 7 - 9) are excellent for deuteron production, but under-estimate the triton and helion data.

5 Summary and Conclusions

Previous work [13, 14] has shown that light ions and neutrons provide the dominant contribution to space radiation dose equivalent for realistic spacecraft shielding of the order of 20 g/cm^2 or more. Because light ions are so important, one would think that the relevant physics needed for space radiation is well characterized. However, comparisons of light ion production among different transport codes and with experimental measurements show significant discrepancies [15, 16, 17]. In fact, light ion production represents the largest physics uncertainty in space radiation studies. Fortunately, the largest discrepancies are in energy regions that make smaller contributions to dose equivalent, and so model predictions of dose equivalent remain reasonably accurate. However, dose equivalent is not the only quantity of interest in space radiation studies, and it is prudent to try to resolve remaining physics and transport discrepancies. Because of their relatively light mass compared to heavy fragment production, light ions and neutrons are scattered at both small and large angles when produced from high energy cosmic ray interactions. Therefore, fully three-dimensional transport methods [4, 5, 6, 7, 8] are required, and consequently, accurate double-differential cross section models are needed for input into 3-dimensional transport codes. Fast and efficient transport codes are used in space radiation studies and consequently efficient cross section parameterization models are desired.

A summary of the work presented in this paper follows:

- A thermal model parameterization for proton production was developed, with the important feature that all three sources of projectile, central fireball and target production of protons was included. This feature was able to explain the distinctive low-momentum, intermediate angle shoulder region in the proton spectrum.

- The three-source proton thermal model was used as input into the coalescence model, to arrive at a cross section model parameterization for light ion production, which also includes the three sources, and are seen to be essential in explaining the light ion shoulders, which are even more pronounced than the proton shoulders.

- The cross section model developed herein represents a very efficient parameterization of proton and light ion double-differential cross sections that can be used efficiently in space radiation transport codes for large angle light ion fragment production.

- Overall, both SHIELD and the parameterization model compare quite well to the majority of the experimental data. SHIELD comparisons to proton production data are excellent and are generally better than the parameterization model. For composite light ion production, both SHIELD and the parameterization model compare well to the majority of the data, except with both producing under-prediction of tritons and helions from C+C reactions, and alpha particles from Ar + KCl reactions at large angles. While the exact cause of these remaining disagreements is unclear, it may be due to the parameters used in the proton thermal model, and the values of the coalescence coefficients for the light ion model. Comparison and detailed parameter fitting to a wider data set, as well as a more accurate theory of coalescence coefficients, may improve some of the remaining discrepancies.

The most important future work, currently underway, involves developing a parameterization model that includes direct channel production of light ions at very small angles, between 0° - 10°. The data in this region show a large quasileastic peak, which needs to be correctly modeled and parameterized. Also, the models need to be compared to data with light ion projectiles. The newly developed models will then be compared to a more extensive data set [27, 30, 51, 52, 53, 54, 55, 56], that includes small angle data and light ion projectiles.

Acknowledgments We wish to thank Drs. Charles Werneth, Ryan Norman, Francis Badavi, and Steve Smith for reviewing the manuscript. Norbury was supported by the Advanced Exploration Systems (AES) Division under the Human Exploration and Operations Mission Directorate of NASA.

Reaction	σ (b)
Ar (800 MeV/n) + KCl $\rightarrow$ p + X	16
C (800 MeV/n) + C $\rightarrow$ p + X	3.5

Table 1: Total strong interaction cross sections calculated from NUCFRG3 [24] used in the parameterized proton thermal model.

Participant (Central Fireball) Temperature	$\Theta_{\mathcal{C}}$	110 MeV
Spectator (Projectile = Target) Temperature	$\Theta_{\mathcal{P}} = \Theta_{\mathcal{T}}$	35 MeV

Table 2: Temperature parameters used in the parameterized proton thermal model.

		^{2}H		^{3}H		^{3}He		^{4}He	
Kinetic Energy (MeV/n)	Reaction	C_A	R (fm)	C_A	R (fm)	C_A	R (fm)	C_A	R (fm)
400	Ne+NaF	1.4×10^{-5}	3.5	1.3×10^{-10}	3.1	8.0×10^{-11}	3.3		
		1.0×10^{-5}	3.3	0.6×10^{-10}	2.9	0.6×10^{-10}	2.9	9.3×10^{-16}	2.3
	Ne+Cu	8.0×10^{-6}	3.7	5.0×10^{-11}	3.2	3.0×10^{-11}	3.4		
		8.1×10^{-6}	3.6	3.6×10^{-11}	3.2	3.6×10^{-11}	3.2	3.1×10^{-16}	2.6
	Ne+Pb	4.4×10^{-6}	4.1	1.3×10^{-11}	3.7	0.6×10^{-11}	3.9		
		5.6×10^{-6}	4.1	1.6×10^{-11}	3.7	1.6×10^{-11}	3.7	7.2×10^{-17}	3.1
800	C+C	3.0×10^{-5}	3.1	6.0×10^{-10}	2.8	6.0×10^{-10}	2.8		
		1.3×10^{-5}	3.1	1.0×10^{-10}	2.7	1.0×10^{-10}	2.7	2.2×10^{-15}	2.1
	C+Pb	6.0×10^{-6}	3.9	2.5×10^{-11}	3.5	1.5×10^{-11}	3.5		
		6.1×10^{-6}	4.0	1.9×10^{-11}	3.6	1.9×10^{-11}	3.6	9.7×10^{-17}	3.0
800	Ne+NaF	1.6×10^{-5}	3.3	2.1×10^{-10}	2.8	1.6×10^{-10}	3.0		
		1.0×10^{-5}	3.3	0.6×10^{-10}	2.9	0.6×10^{-10}	2.9	9.3×10^{-16}	2.3
	Ne+Cu	8.0×10^{-6}	3.7	5.0×10^{-11}	3.2	4.0×10^{-11}	3.3		
		8.1×10^{-6}	3.6	3.6×10^{-11}	3.2	3.6×10^{-11}	3.2	3.1×10^{-16}	2.6
	Ne+Pb	4.0×10^{-6}	4.2	1.2×10^{-11}	3.7	0.6×10^{-11}	3.9		
		5.6×10^{-6}	4.1	1.6×10^{-11}	3.7	1.6×10^{-11}	3.7	7.2×10^{-17}	3.1
800	Ar+KCl	8.0×10^{-6}	3.5	3.5×10^{-11}	3.2	3.5×10^{-11}	3.2	3.0×10^{-16}	2.8
		8.0×10^{-6}	3.6	3.5×10^{-11}	3.2	3.5×10^{-11}	3.2	3.0×10^{-16}	2.6
	Ar+Pb	3.0×10^{-6}	4.3	0.9×10^{-11}	3.6	0.5×10^{-11}	3.7	3.0×10^{-17}	3.0
		5.0×10^{-5}	4.2	1.2×10^{-11}	3.8	1.2×10^{-11}	3.8	4.4×10^{-17}	3.2
2100	Ne+NaF	1.4×10^{-5}	3.5	0.5×10^{-10}	3.6	0.5×10^{-10}	3.6		
		1.0×10^{-5}	3.3	0.6×10^{-10}	2.9	0.6×10^{-10}	2.9	9.3×10^{-16}	2.3
	Ne+Pb	4.0×10^{-6}	4.2	0.6×10^{-11}	4.2	0.3×10^{-11}	4.4		
		5.6×10^{-6}	4.1	1.6×10^{-11}	3.7	1.6×10^{-11}	3.7	7.2×10^{-17}	3.1

Table 3: Coalescence coefficients, C_A, and interaction radii, R, observed (first row in each box) and calculated (second row in each box). All observed values are taken from Table VIII of reference [26], although many values for ^{4}He are missing. Calculations of C_A and R use equations (21) and (22), respectively.

	^{2}H	^{3}H	^{3}He	^{4}He
c_A	1.6×10^{-3}	6.9×10^{-7}	6.9×10^{-7}	1.3×10^{-10}

Table 4: Constant c_A determined from equation (23), and used for calculation of the coalescence coefficient, C_A, given in equation (21).

Reactions	Fragments	Angles (degrees)
Ar (800 MeV/n) + KCl	Proton	10, 15, 20, 30, 40, 50, 60, 70, 80, 90, 100, 110, 145
	Deuteron	10, 30, 60, 80, 110, 145
	Triton	15, 30, 60, 80, 110, 145
	Helion	15, 30, 60, 80
	Alpha	15, 30, 60, 80
C (800 MeV/n) + C	Proton	15, 45, 70, 145
	Deuteron	15, 45, 70, 145
	Triton	15, 45, 70
	Helion	15, 45, 70

Table 5: Summary of 47 data sets studied. Each data set contains an average of 24 points, so that the total number of data points studied is over 1,000.

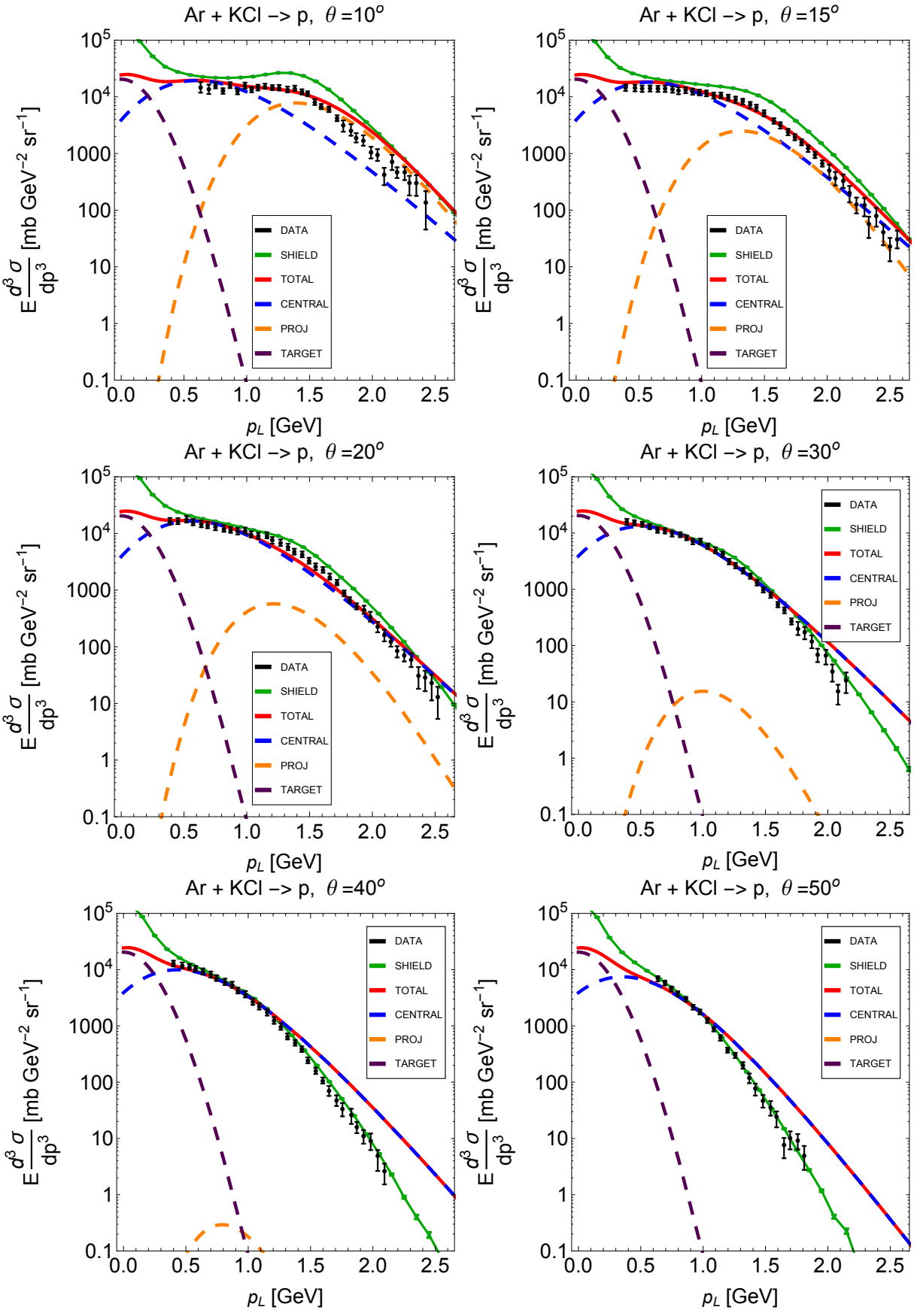


Figure 1: Parameterized proton thermal model and SHIELD cross sections at various production angles as a function of lab momentum for Ar + KCl reactions compared to experimental data [26]. Total (red) and individual contributions from central fireball (blue), projectile (orange), and target (purple) are shown for the parameterized model. The individual contributions simply add to give the total, as in equation (18). Figure is continued on the next page.

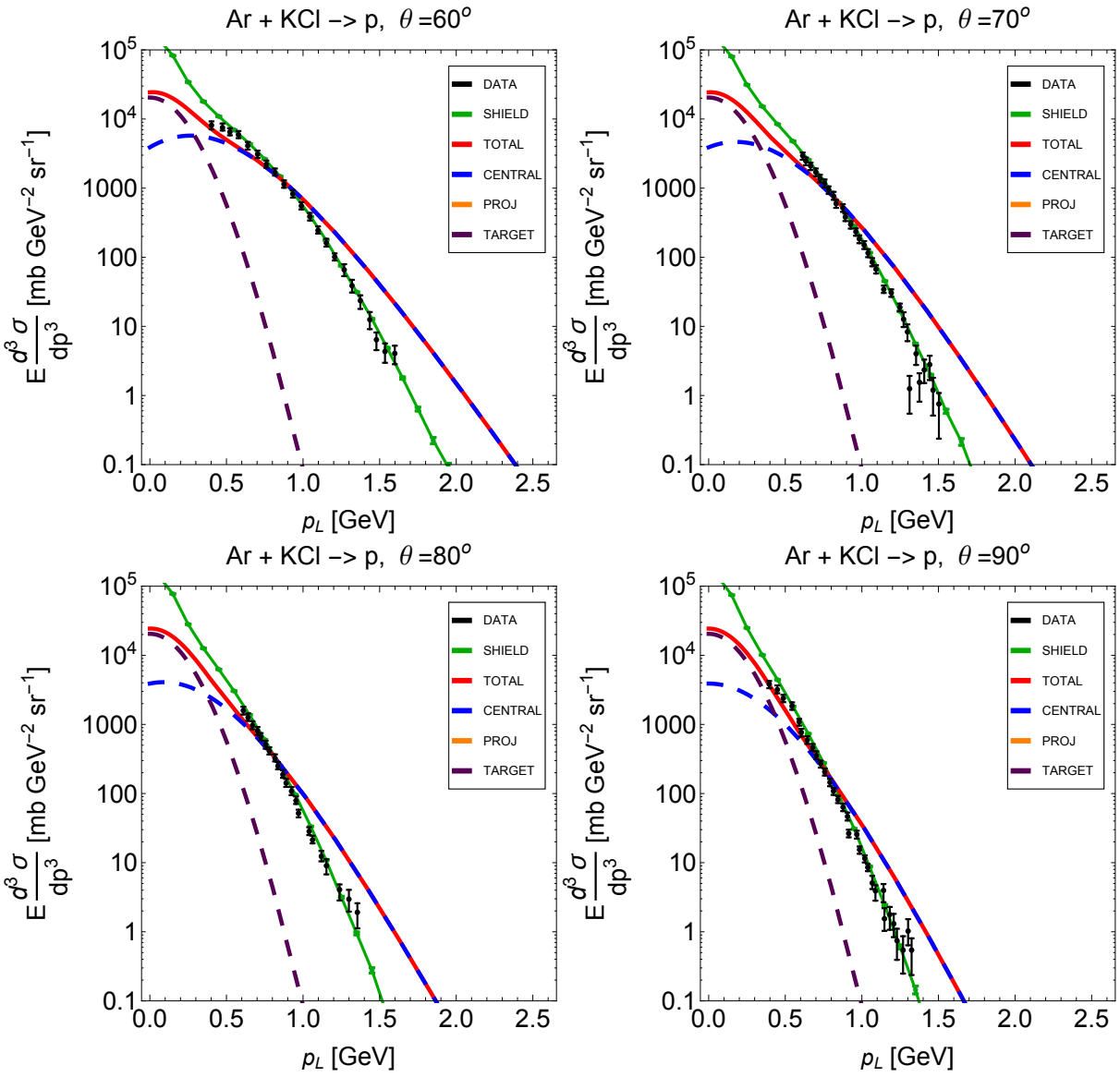


Figure 1 continued from previous page. Figure is also continued on the next page.

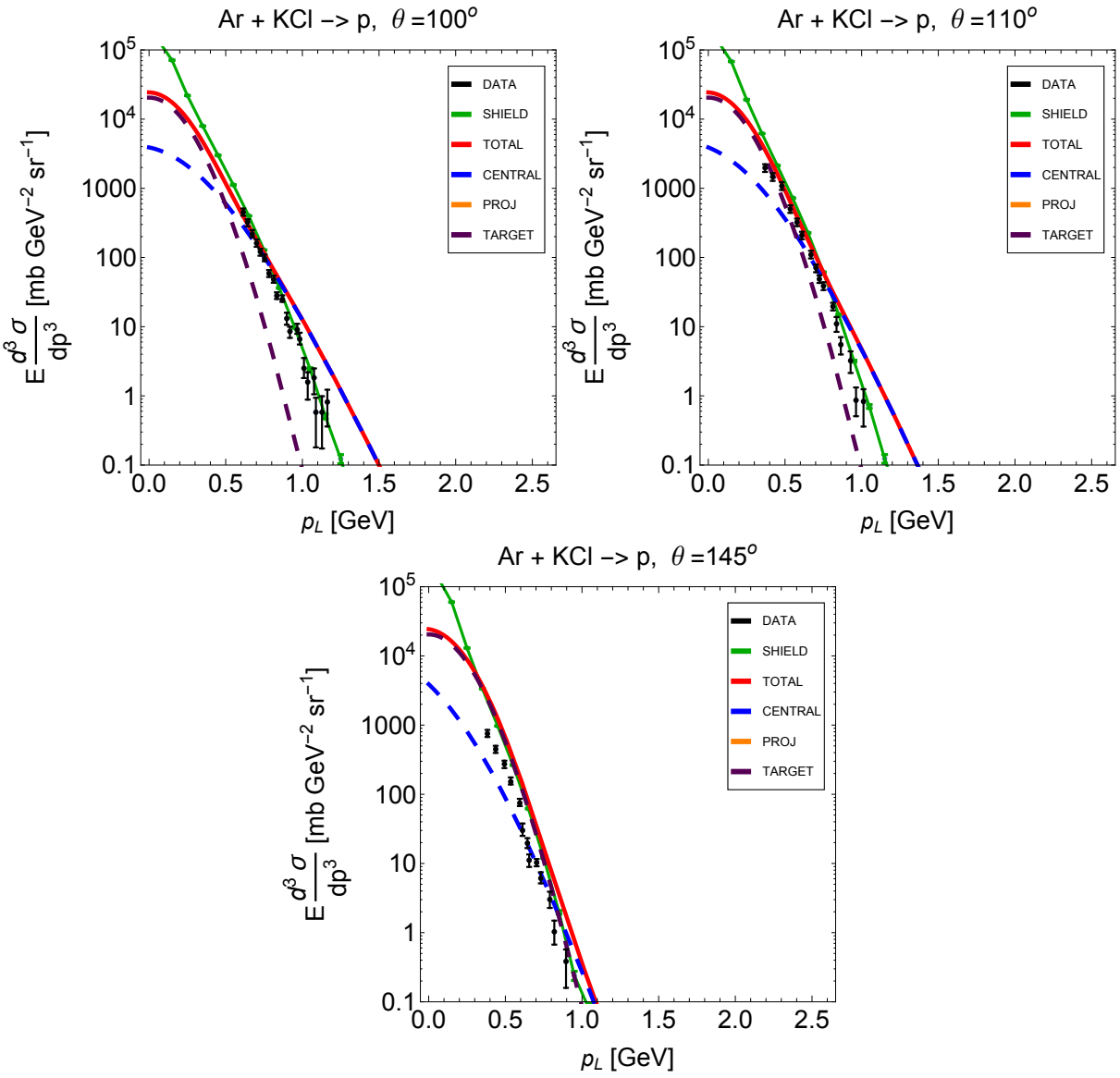


Figure 1 continued from previous page.

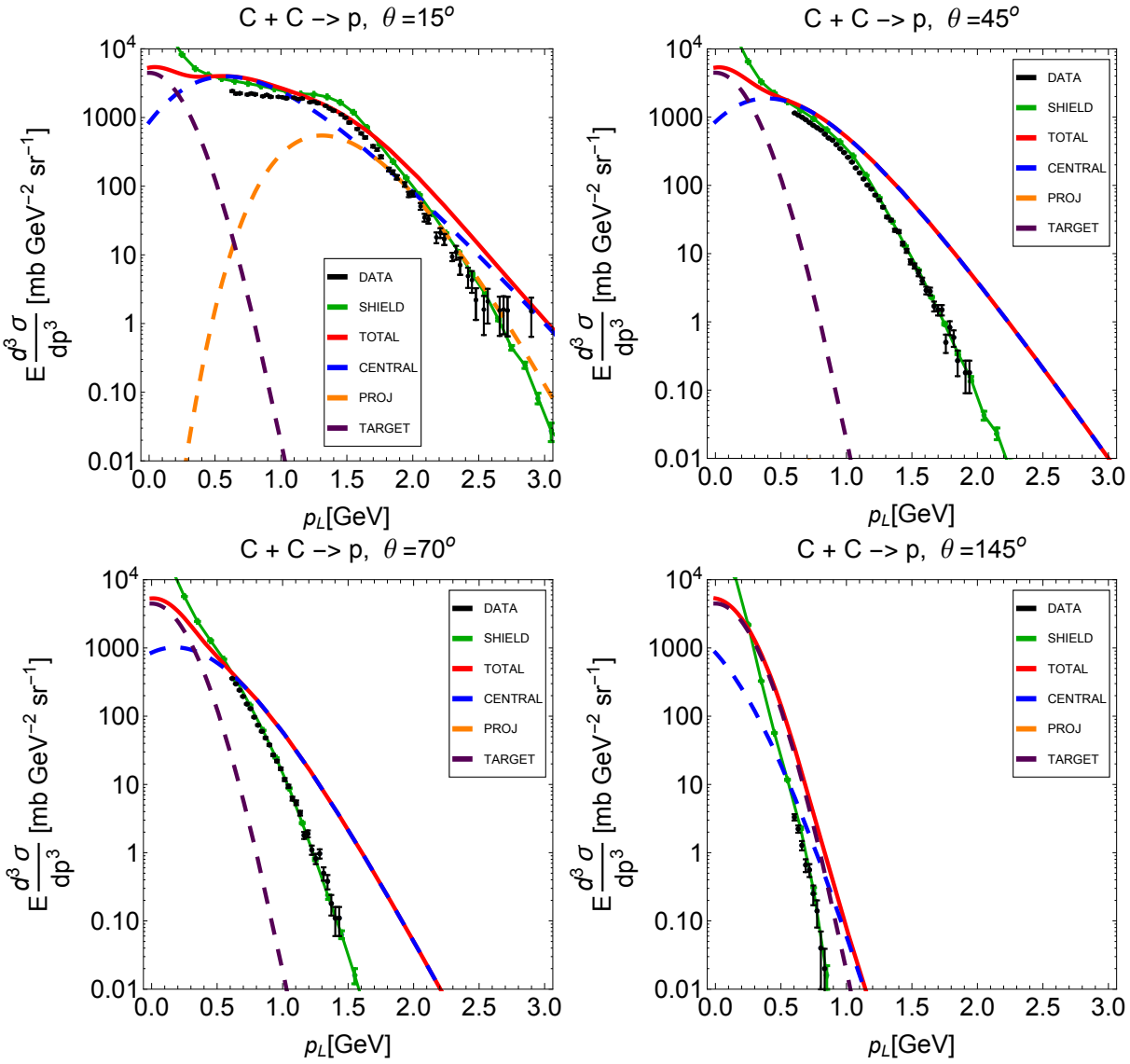


Figure 2: Parameterized proton thermal model and SHIELD cross sections at various production angles as a function of lab momentum for C + C reactions compared to experimental data [57]. Total (red) and individual contributions from central fireball (blue), projectile (orange), and target (purple) are shown for the parameterized model. The individual contributions simply add to give the total, as in equation (18).

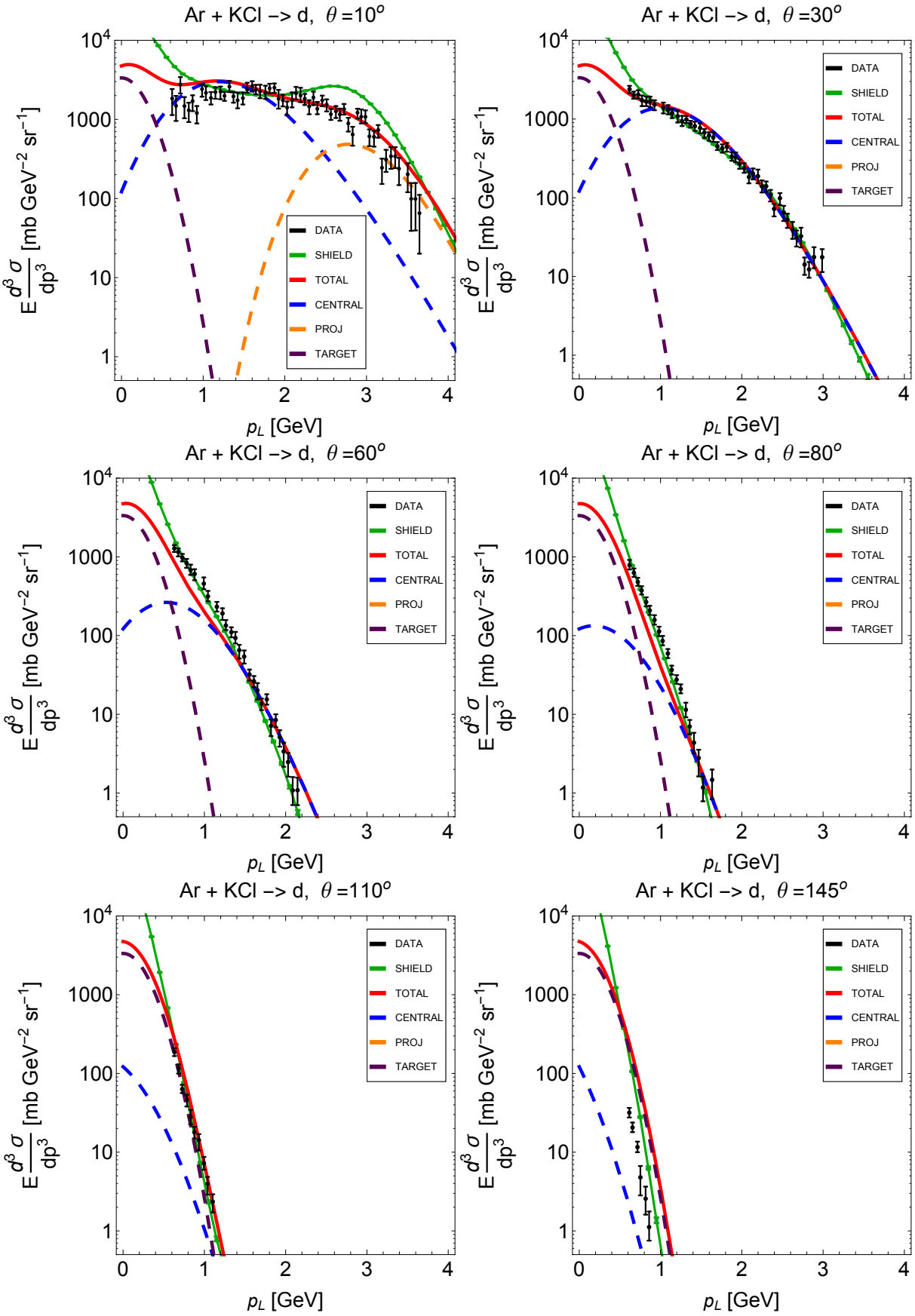


Figure 3: Parameterized deuteron coalescence model and SHIELD cross sections at various production angles as a function of lab momentum for Ar + KCl reactions compared to experimental data [26]. Total (red) (equation 20) and separated (equation 19) contributions from central fireball (blue), projectile (orange), and target (purple) are shown for the parameterized model. Rather than a simple addition, individual contributions add according to equation (20).

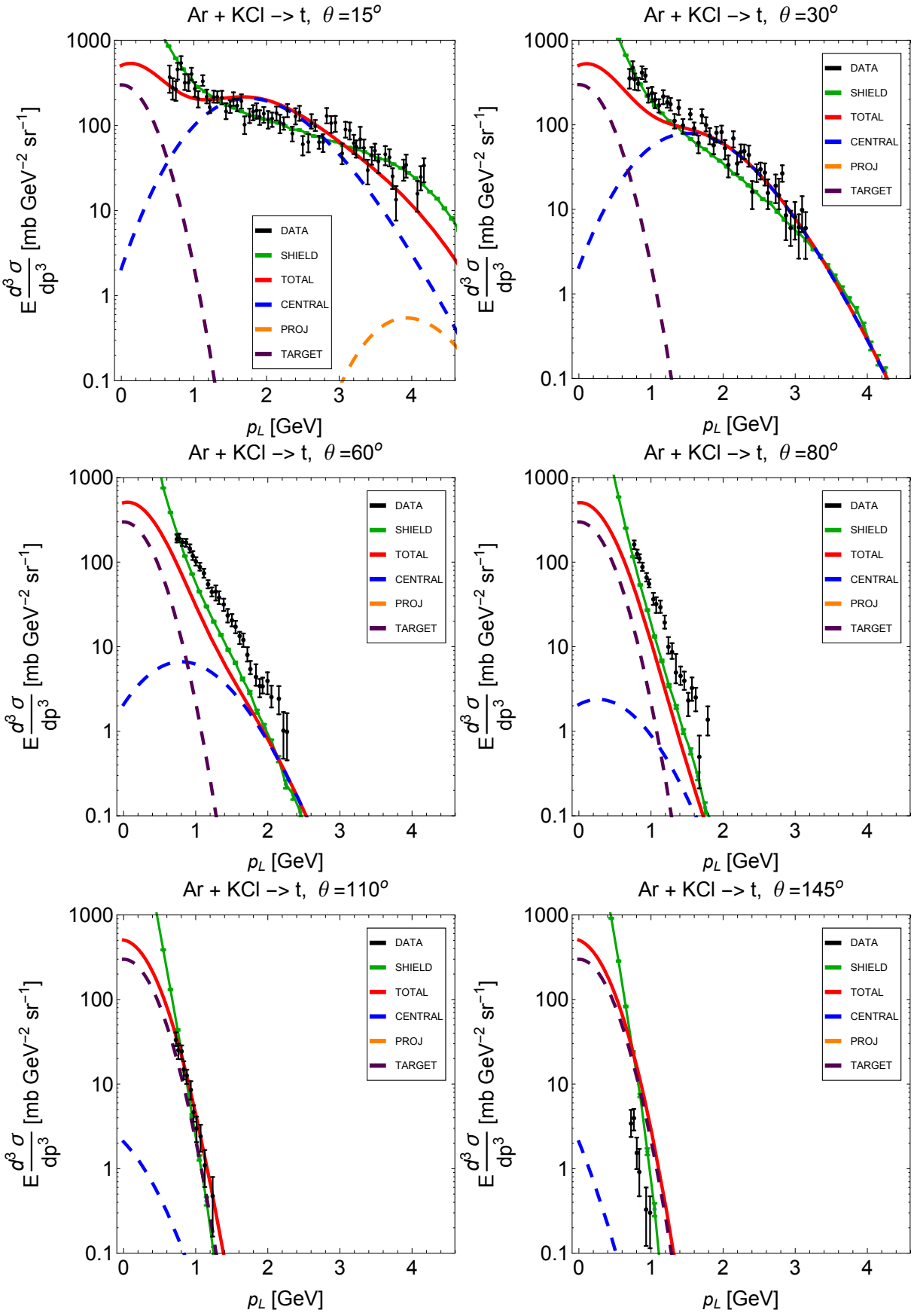


Figure 4: Parameterized triton coalescence model and SHIELD cross sections at various production angles as a function of lab momentum for Ar + KCl reactions compared to experimental data [26]. Total (red) (equation 20) and separated (equation 19) contributions from central fireball (blue), projectile (orange), and target (purple) are shown for the parameterized model. Rather than a simple addition, individual contributions add according to equation (20).

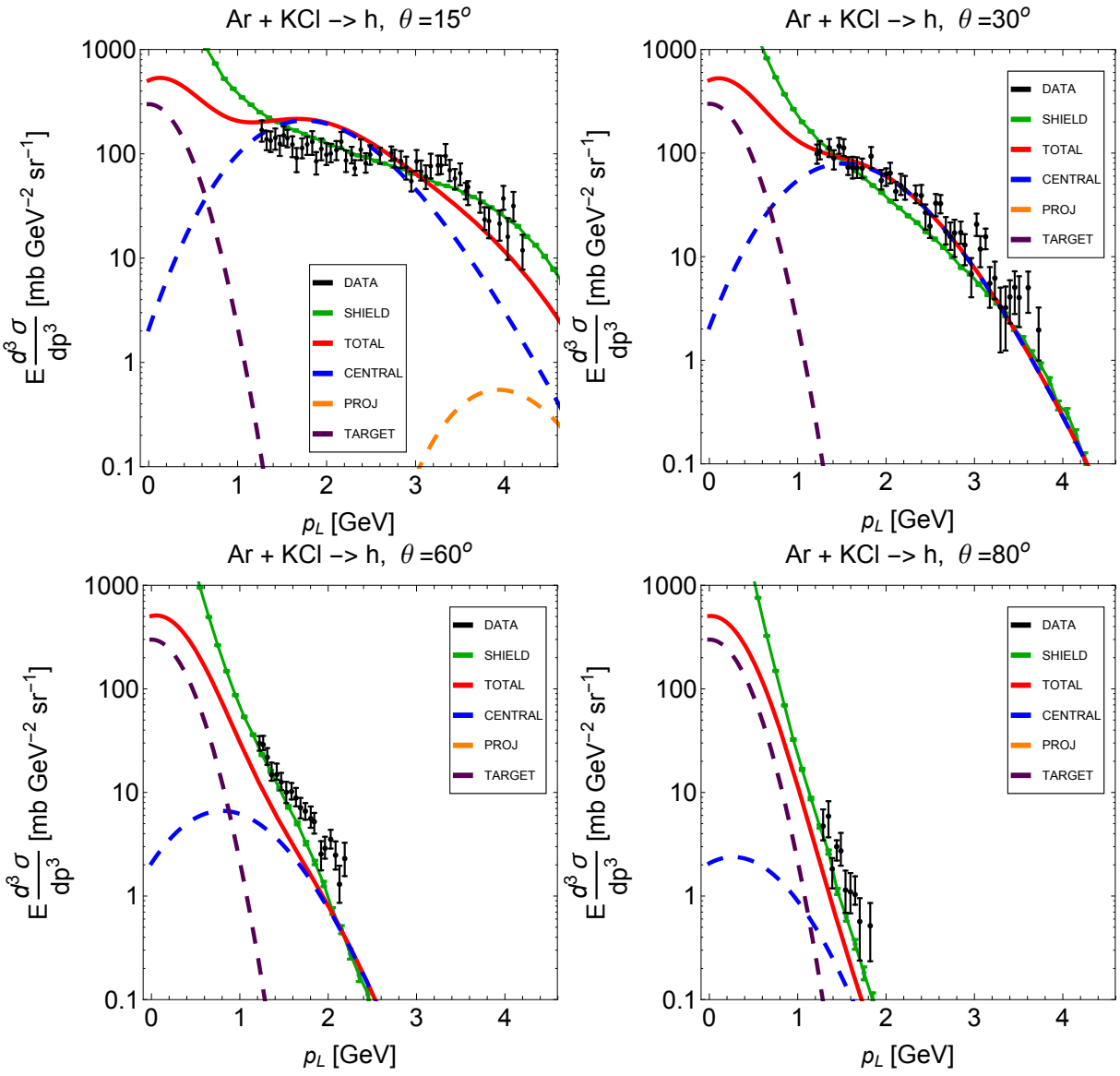


Figure 5: Parameterized helion coalescence model and SHIELD cross sections at various production angles as a function of lab momentum for Ar + KCl reactions compared to experimental data [26]. Total (red) (equation 20) and separated (equation 19) contributions from central fireball (blue), projectile (orange), and target (purple) are shown for the parameterized model. Rather than a simple addition, individual contributions add according to equation (20).

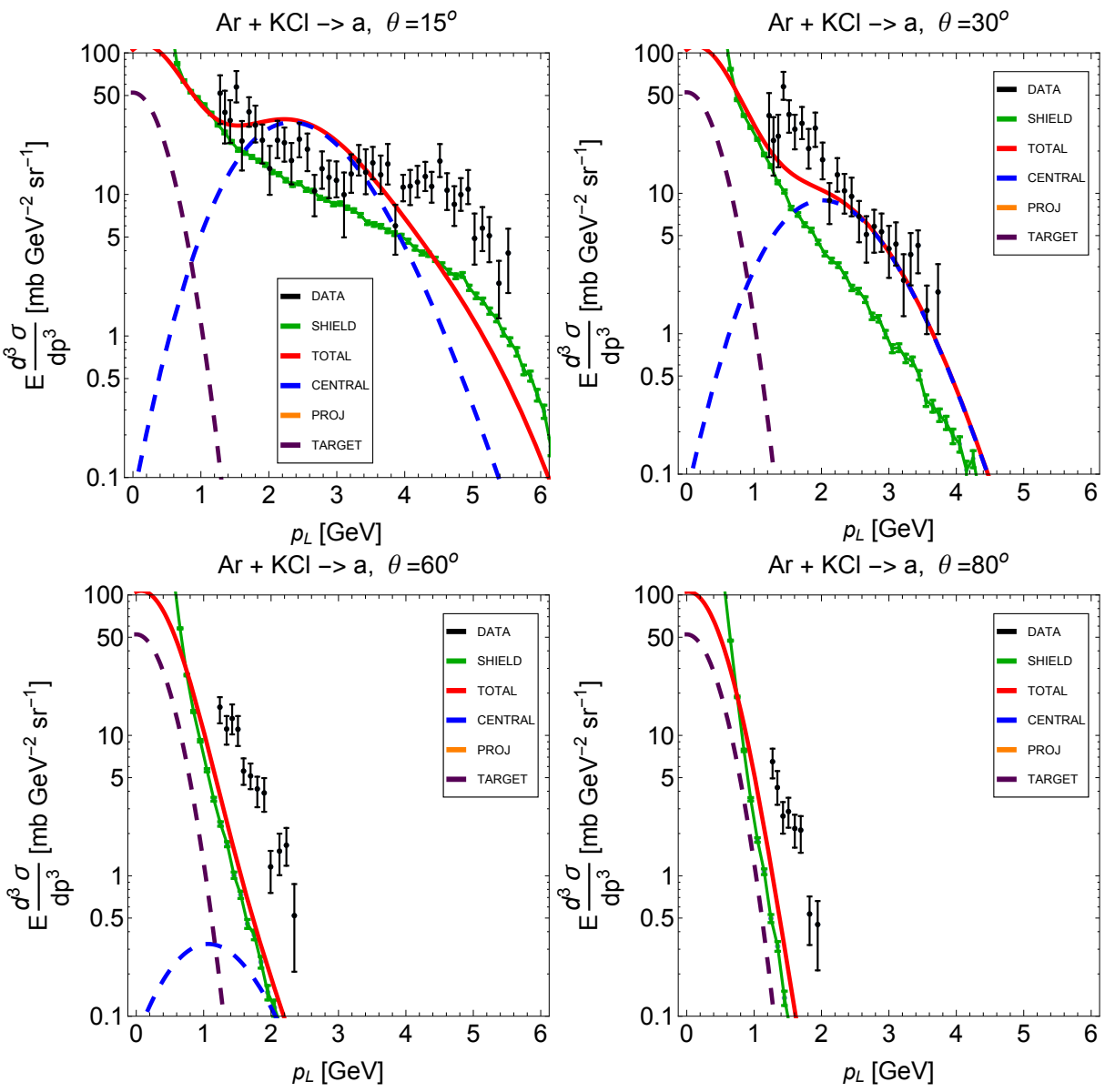


Figure 6: Parameterized alpha coalescence model and SHIELD cross sections at various production angles as a function of lab momentum for Ar + KCl reactions compared to experimental data [26]. Total (red) (equation 20) and separated (equation 19) contributions from central fireball (blue), projectile (orange), and target (purple) are shown for the parameterized model. Rather than a simple addition, individual contributions add according to equation (20).

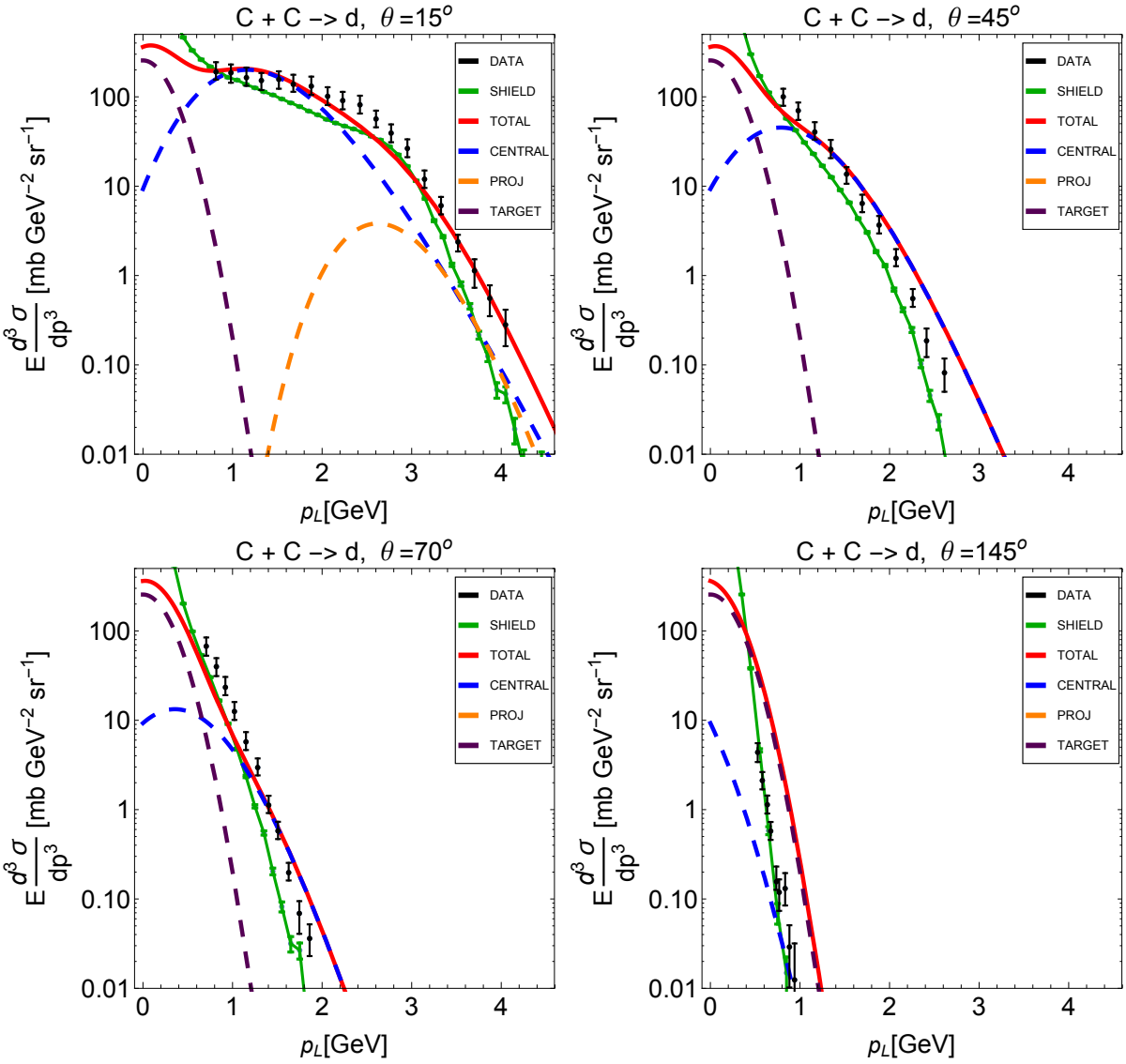


Figure 7: Parameterized deuteron coalescence model and SHIELD cross sections at various production angles as a function of lab momentum for C + C reactions compared to experimental data [26]. Total (red) (equation 20) and separated (equation 19) contributions from central fireball (blue), projectile (orange), and target (purple) are shown for the parameterized model. Rather than a simple addition, individual contributions add according to equation (20).

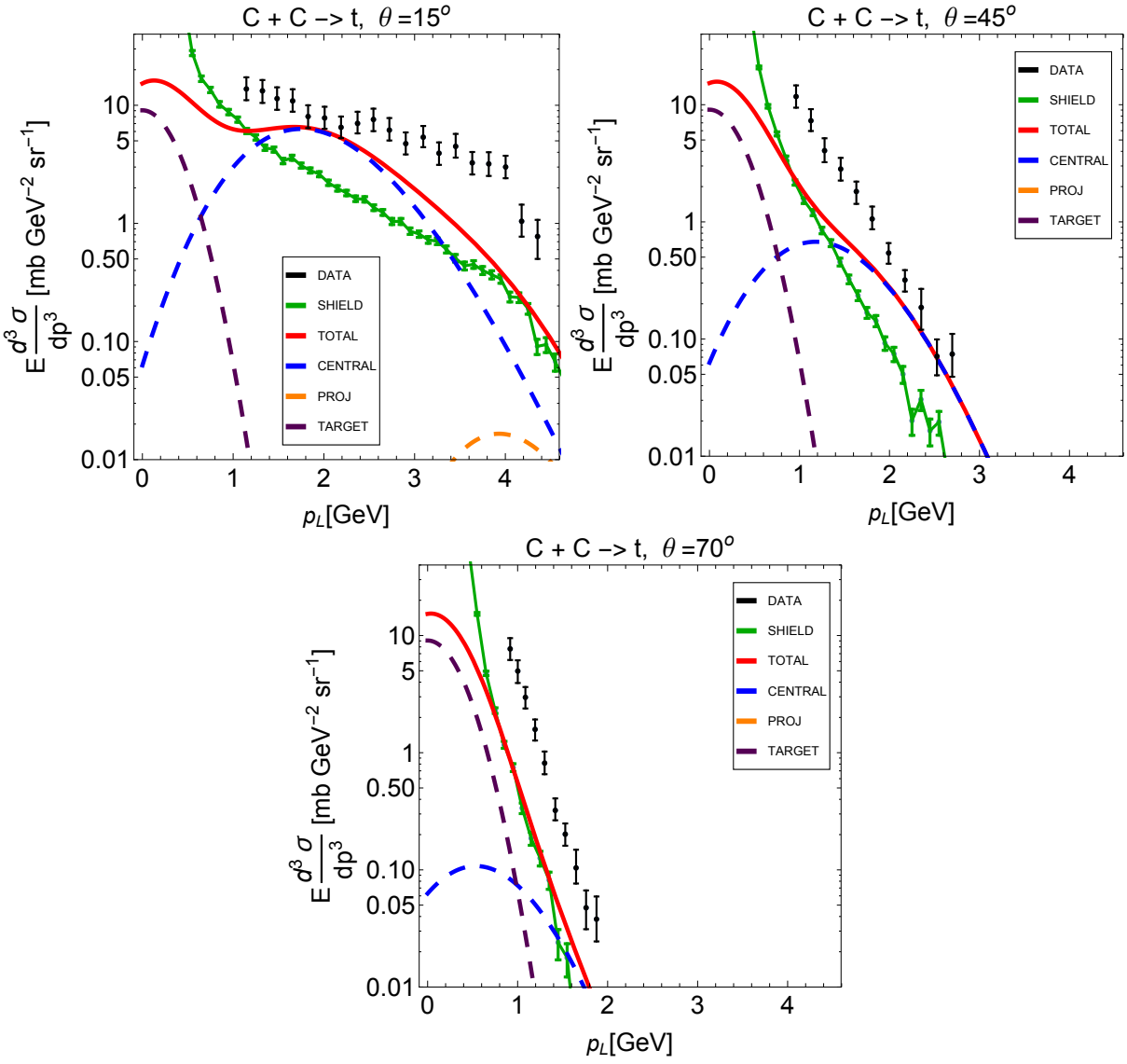


Figure 8: Parameterized triton coalescence model and SHIELD cross sections at various production angles as a function of lab momentum for C + C reactions compared to experimental data [26]. Total (red) (equation 20) and separated (equation 19) contributions from central fireball (blue), projectile (orange), and target (purple) are shown for the parameterized model. Rather than a simple addition, individual contributions add according to equation (20).

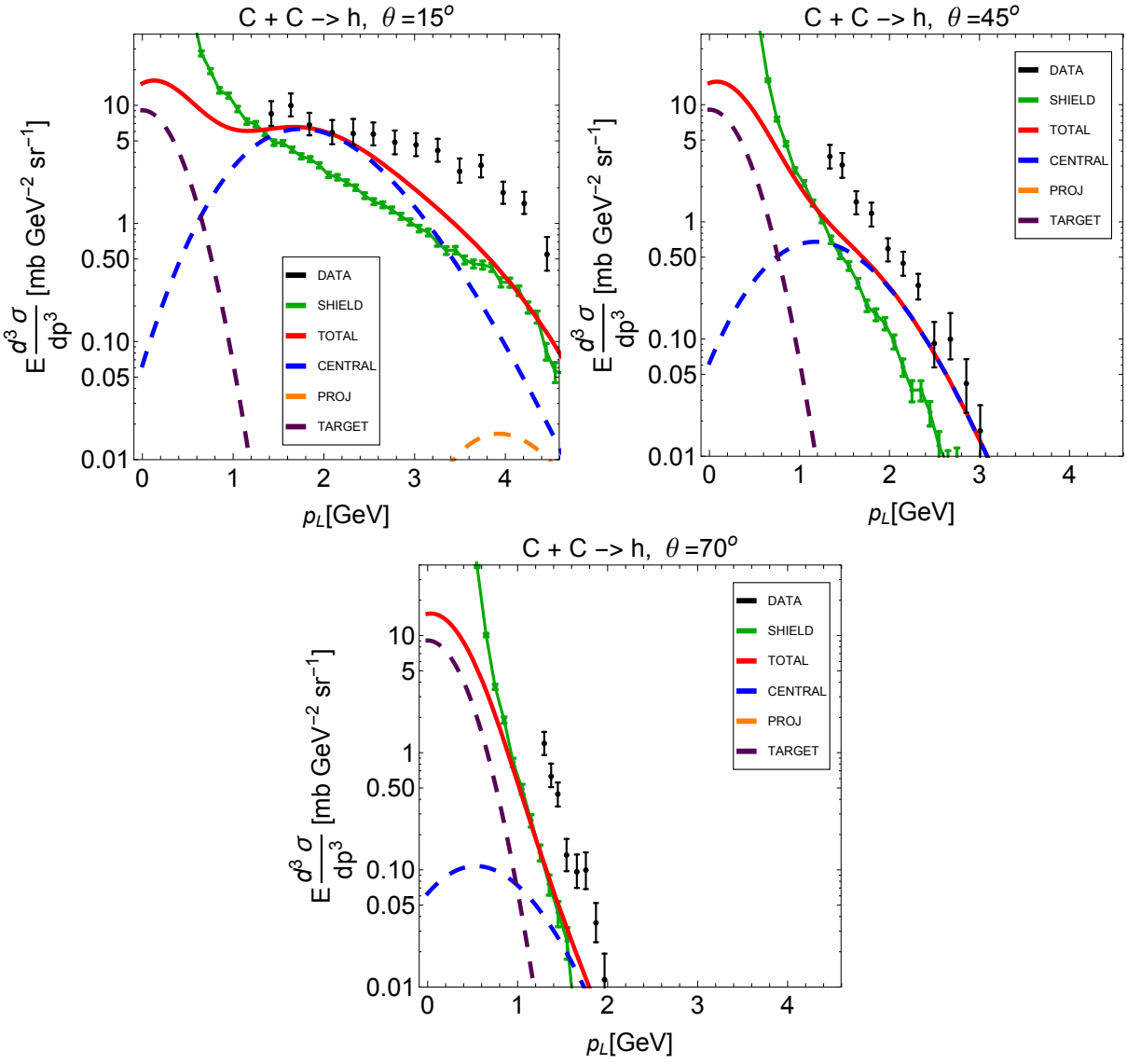


Figure 9: Parameterized helion coalescence model and SHIELD cross sections at various production angles as a function of lab momentum for C + C reactions compared to experimental data [26]. Total (red) (equation 20) and separated (equation 19) contributions from central fireball (blue), projectile (orange), and target (purple) are shown for the parameterized model. Rather than a simple addition, individual contributions add according to equation (20).

References

[1] J.W. Norbury, T.C. Slaba, N. Sobolevsky, B. Reddell, Life Sci. Space Res. 14 (2017) 64.

[2] J.W. Norbury, N., Sobolevsky, C.M. Werneth, Nucl. Instr. Meth. Phys. Res. B 418 (2018) 13.

[3] J.W. Norbury, K. Whitman, K. Lee, T.C. Slaba, F.F. Badavi, Life Sci. Space Res. 18 (2018) 64.

[4] J.W. Wilson, T.C. Slaba, F.F. Badavi, B.D. Reddell, A.A. Bahadori, Life Sci. Space Res. 2 (2014) 6.

[5] J.W. Wilson, T.C. Slaba, F.F. Badavi, B.D. Reddell, A.A. Bahadori, Life Sci. Space Res. 4 (2015) 46.

[6] J.W. Wilson, T.C. Slaba, F.F. Badavi, B.D. Reddell, A.A. Bahadori, Life Sci. Space Res. 7 (2015) 27.

[7] J.W. Wilson, T.C. Slaba, F.F. Badavi, B.D. Reddell, A.A. Bahadori, Life Sci. Space Res. 9 (2016) 69.

[8] T.C. Slaba, J.W. Wilson, F.F. Badavi, B.D. Reddell, A.A. Bahadori, Life Sci. Space Res. 9 (2016) 77.

[9] A.V. Dementyev, N.M. Sobolevsky, Rad. Meas. 30 (1999) 553.

[10] D.C. Hansen, A. Luhr, N. Sobolevsky, N. Bassler, Phys. Med. Biol. 57 (2012) 2392.

[11] G. Battistoni et al., Ann. Nucl. Energy 82 (2015) 10.

[12] S. Agostinelli et al., Nucl. Instr. Meth. Phys. Res. A 506 (2003) 250.

[13] J.W. Norbury, T.C. Slaba, Life Sci. Space Res. 3 (2014) 90.

[14] S.A. Walker, L.W. Townsend, J.W. Norbury, Adv. Space Res. 51 (2013) 1792.

[15] T.C. Slaba, A.A. Bahadori, B.D. Reddell, R.C. Singleterry, M.S. Clowdsley, S.R. Blattnig, Life Sci. Space Res. 12 (2017) 1.

[16] D. Matthia et al., J. Space Weath. Space Clim. 6 (2016) A13.

[17] L.H. Heilbronn, private communication (2018). Work to be published soon.

[18] T. Sato, K. Niita, H. Iwase, H. Nakashima, Y. Yamaguchi, L. Sihver, Rad. Meas. 41 (2006) 1142.

[19] T. Sato et al., J. Nucl. Sci. Technol. 50 (2013) 913.

[20] G.W. McKinney, D.J. Lawrence, T.H. Prettyman, R.C. Elphic, W.C. Feldman, J.J. Hagerty, J. Geophys. Res. 111 (2006) E06004.

[21] Y.M. Charara, L.W. Townsend, T.A. Gabriel, C.J. Zeitlin, L.H. Heilbronn, J. Miller, IEEE Trans. Nucl. Sci. 55 (2008) 3164.

[22] L.W. Townsend, T.M. Miller, T.A. Gabriel, Rad. Prot. Dosim. 116 (2005) 135.

[23] J.W. Wilson, L.W. Townsend, W. Schimmerling, G.S. Khandelwal, F. Khan, J.E. Nealy, F.A. Cucinotta, L.C. Simonsen, J.L. Shinn, J.W. Norbury, NASA Reference Publication 1257 (1991). https://www.sti.nasa.gov

[24] A.M. Adamczyk, R.B. Norman, S. Sriprisan, L.W. Townsend, J.W. Norbury, S.R. Blattnig, T.C. Slaba, Nucl. Instr. Meth. Phys. Res. A 678 (2012) 21.

[25] R.L. Auble, Phys. Rev. C 28 (1983) 1552.

[26] S. Nagamiya, M.C. Lemaire, E. Moeller, S. Schnetzer, G. Shapiro, H. Steiner, I. Tanihata, Phys. Rev. C 24 (1981) 971.

[27] L. Anderson, W. Bruckner, E. Moeller, S. Nagamiya, S. Nissen-Meyer, L. Schroeder, G. Shapiro, H. Steiner, Phys. Rev. C 28 (1983) 1224.

[28] J.W. Norbury, NASA Technical Publication 2018-220077. https://www.sti.nasa.gov.

[29] G.D. Westfall, J. Gossett, P.J. Johansen, A.M. Poskanzer, W.G. Meyer, H.H. Gutbrod, A. Sandoval, R. Stock, Phys. Rev. Lett. 37 (1976) 1202.

[30] J. Gosset, H.H. Gutbrod, W.G. Meyer, A.M. Poskanzer, A. Sandoval, R. Stock, G.D. Westfall, Phys. Rev. C 16 (1977) 629.

[31] M.R. Spiegel, Mathematical Handbook, Schaum's Outline Series, McGraw-Hill, New York, p. 141, 1968.

[32] J.W. Norbury, F. Dick, NASA Technical Publication 2008-215543. https://www.sti.nasa.gov.

[33] T. Nakamura, L. Heilbronn, Handbook on secondary particle production and transport by high-energy heavy ions, World Scientific, Singapore, 2006.

[34] T.C. Awes, G. Poggi, S. Saini, C.K. Gelbke, R. Legrain, G.D. Westfall, Phys. Lett. B 103 (1981) 417.

[35] B.A. Remington, G. Caskey, A. Galonsky, C.K. Gelbke, L. Heilbronn, J. Heltsley, M.B. Tsang, F. Deak, A. Kiss, Z. Seres, J. Kasagi, J.J. Kolata, Phys. Rev. C 34 (1986) 1685.

[36] H.R. Schelin, A. Galonsky, C.K. Gelbke, H. Hama, L. Heilbronn, D. Krofcheck, W. Lynch, D. Sackett, M.B. Tsang, X. Yang, F. Deak, A. Horvath, A. Kiss, Z. Seres, J. Kasagi, T. Murakami, Nucl. Sci. Eng. 113 (1993) 184.

[37] T. Kato, T. Kurosawa, T. Nakamura, Nucl. Instr. Meth. Phys. Res. A 480 (2002) 571.

[38] Y. Iwata, T. Murakami, H. Sato, H. Iwase, T. Nakamura, T. Kurosawa, L. Heilbronn, R.M. Ronningen, K. Ieki, Y. Tozawa, K. Niita, Phys. Rev. C 64 (2001) 054609.

[39] J.W. Norbury, A.M. Adamczyk, Nucl. Instr. Meth. Phys. Res. B 254 (2007) 177.

[40] J.W. Norbury, Nucl. Instr. Meth. Phys. Res. A 703 (2013) 220.

[41] A.S. Botvina, A.V. Dementyev, O.N. Smirnova, N.M. Sobolevsky, V.D. Toneev, MSDM - multi stage dynamical model. International codes and model intercomparison for intermediate energy activation yields. In: R.R. Michel and P.P. Nagel, (Eds.), NSC/DOC(97)-1, NEA/P & T No 14, OECD, Paris, 1997, p. 307.

[42] V.D. Toneev, K.K. Gudima, Nucl. Phys. A 400 (1983) 173c.

[43] N.S. Amelin, K.K. Gudima, V.D. Toneev, Yadernaya Fizika 51 (1990) 1730 (in Russian). Preprint GSI-89-52 (in English).

[44] N.S. Amelin, K.K. Gudima, S.Y. Siviklokov, V.D. Toneev, Yadernaya Fizika 52 (1990) 272 (in Russian).

[45] K.K. Gudima, S.G. Mashnik, V.D. Toneev, Nucl. Phys. A 401 (1983) 329.

[46] A.S. Botvina, A.S. Iljinov, I.N. Mishustin, J.P. Bondorf, R. Donangelo, K. Sneppen, Nucl. Phys. A 475 (1987) 663.

[47] G.D. Adeev, A.S. Botvina, A.S. Iljinov, M.V. Mebel, N.I. Piscasov, O.I. Serdyuk, A method of calculation of mass and energy distributions of fission residuals in reactions induced by intermediate energy particles. Preprint INR RAS 816/1993, Moscow (in Russian), (1993).

[48] J.P. Bondorf, A.S. Botvina, A.S. Iljinov, I.N. Mishustin, K. Sneppen, Phys. Rep. 257 (1995) 133.

[49] J.W. Norbury, Phys. Rev. C 79 (2009) 037901.

[50] C.M. Werneth, J.W. Norbury, S.R. Blattnig, Nucl. Instr. Meth. Phys. Res. B 298 (2013) 86.

[51] H.H. Gutbrod, A. Sandoval, P.J. Johansen, A.M. Poskanzer, J. Gosset, W.G. Meyer, G.D. Westfall, R. Stock, Phys. Rev. Lett. 37 (1976) 667.

[52] J. Banaigs, et al., Phys. Rev. C 35 (1987) 1416.

[53] M.C. Lemaire, S. Nagamiya, S. Schnetzer, H. Steiner, I. Tanihata, Phys. Lett. B 85 (1979) 38.

[54] T. Motobayashi, H. Ejiri, T. Shibata, K. Okada, M. Sasao, K. Maeda, H. Suzuki, A. Shimizu, H. Sakai, Nucl. Phys. A 413 (1984) 290.

[55] G.D. Westfall et al., Phys. Lett. B 116 (1982) 118.

[56] G.D. Westfall et al., Phys. Rev. C 29 (1984) 861.

[57] M.C. Lemaire, S. Nagamiya, O. Chamberlain, G. Shapiro, S. Schnetzer, H. Steiner, I. Tanihata, Lawrence Berkeley Laboratory report number LBL-8463 (1978).